Manuscript refereed by Gemma Herranz (Universidad de Castilla La Mancha, Spain)

Lithography-based Metal Manufacturing (LMM) of 316L Powder

Authors

Gerald Mitteramskogler*, Martin Schwentenwein*, Carlo Burkhardt**, Nick Cruchley***

[*] Dr. G. Mitteramskogler, Dr. M. Schwentenwein. Lithoz GmbH.
Mollardgasse 85a/2/64-69. 1060 Vienna (Austria). gmitteramskogler@lithoz.com
mschwentenwein@lithoz.com

[**] Prof. Dr. C. Burkhardt. Pforzheim University of Applied Sciences
Tiefenbronner Str. 65 75175 Pforzheim (Germany). carlo.burkhardt@hs-pforzheim.de

[***] Dr. Nick Cruchley. MTC Limited
Ansty Business Park. CV7 9JU Coventry (United Kingdom). Nick.cruchley@the-mtc.org

Keywords

Additve Manufacturing, Stereolithography, metal suspension, debinding, sintering, photopolymerisation

Abstract

A vat polymerization-based additive manufacturing processes, called Lithography-based Metal Manufacturing (LMM), has been developed for the manufacturing of metallic green parts. A photoreactive metal-filled feedstock, with a solids loading of up to 50 vol%, is selectively cured by exposure to light. After the layer-by-layer printing process, the green parts require a debinding and sintering step to gain their final metallic properties. This thermal treatment—similar to the thermal treatment used for Metal Injection Molding (MIM)—eliminates polymer binder and is referred to as debinding. As a last step, the debound structure can be sintered up to 98.5 % of the theoretical density of 316L. Using the LMM process, highly complex parts could be manufactured showing a good geometrical accuracy and very low surface roughness. Also the mechanical properties of the AM structure are comparable to conventionally manufactured 316L.

Introduction

The principle of Vat Photopolymerisation (VP) has been successfully commercialized for various types of engineering materials, such as toughness modified photopolymers [1], [2] and ceramics [3]. Among additive manufacturing (AM) techniques, VP-based processes stand out in terms of achievable precision and surface quality [4]. This is because visible or UV light is used as an energy source, which can be projected with great precision by using a high performance projector or a laser scanning unit. An example of an industrial VP-based AM process is called Lithography-based Ceramic Manufacturing (LCM) developed by Lithoz [5]. LCM is an indirect processing route, where the AM machine builds up a so called green parts layer-by-layer. Afterwards the green part is thermally debound to burn off the polymer binder. The remaining chalk-like powder is then sintered close to 100% density to develop the final mechanical properties. The LCM process has proven to achieve a homogeneous, isotropic, and stress-free microstructure after sintering, which is the basis for the manufacturing of functional components [6], [7].

Until now, the benefits of the LCM principle couldn´t be transferred to the processing of metal powders. The LCM principle is suitable for sub-micrometer sized ceramic powder. However, the metal powders are usually two orders of magnitude coarser, which limits the flow ability of the powder when generating a new layer. This results in a nose-cone like structure on top of the printed parts, which builds up until the material vat or the green part is damaged. On the other hand, if the applied layer on the material vat is chosen too thin, air bubbles are trapped inside the green parts, which result in unwanted pores (Figure 1). Another issue with the VP of metal powders concerns the optically “dark” nature of metal powders [8]. Unlike translucent ceramics, the limits the achievable depth of cure, which should be roughly two

times the thickness of the used layers. Because of the mentioned problems, the creation of a new layer is of major importance for the quality of the green parts and the final sintered geometries.

In order to optimize the formation of a new layer a VP-based AM process, called Lithography-based Metal Manufacturing (LMM) was developed. This work characterizes the whole process chain in terms of surface roughness, mechanical properties, microstructure, and chemistry. The parts have been printed by Lithoz, the debinding and sintering was conducted by OBE, the design and the characterization was performed by MTC.

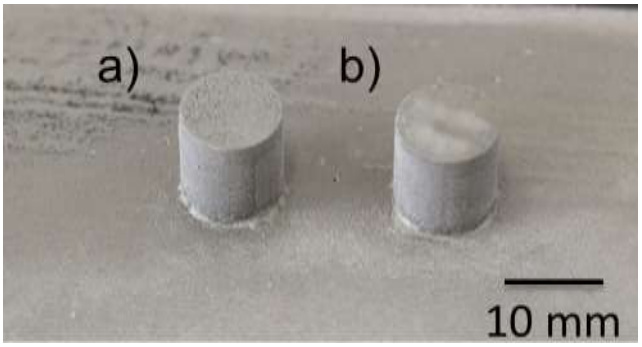

Figure 1 LCM printed green parts on a building platform made of 316L showing pores (a) and a nosecone structure (b)

Materials and Methods

The LMM machine is based on a top-down VP principle. The liquid photo-reactive feedstock is polymerized from above by a high-performance projection unit (Figure 2). The building platform with the submerged green parts is layer-by-layer lowered according to the chosen layer thickness. For this work, a layer thickness of 50 µm was chosen. After the curing of a layer, the wiper blade applies a fresh film of feedstock. The size of the building platform is 75 mm x 43 mm and the resolution in x- and y-direction is 40 µm (HD projector). The printing time of a single layer was 35 s, which results in a build speed of 6 mm/h in z-direction (about 20 cm^3/h in volume).

A photo-reactive feedstock was prepared, based on commercially available di- and polyfunctional methacry-lates (60 wt%). The reactive components include an initiation system, a proprietary photoinitiator, which absorbs light in the wavelengths emitted by the projector. A solid loading of MIM-grade 316L powder up to 50 vol% was achieved. The binder components and the metallic powder were added in a mixing cup and homogeneously dispersed using a SpeedMixer™ laboratory mixer.

The self-supporting function of the material enables the volume-optimized placement of different parts on a single building platform without the need of additional support structures. The only manual operation necessary is to load the parts into the respective program (Netfabb by Autodesk®, or Magics by Materialise). The 3D nesting operation is automatically performed by the software. The job in Figure 3 was generated resulting in a volume occupancy of 70% of the overall building volume.

After the printing process a debinding and sintering stage is required for the parts to gain their final metallic properties. The final parts were evaluated using: Alicona confocal microscopy (roughness) optical microscopy. Mechanical properties were evaluated through tensile testing.

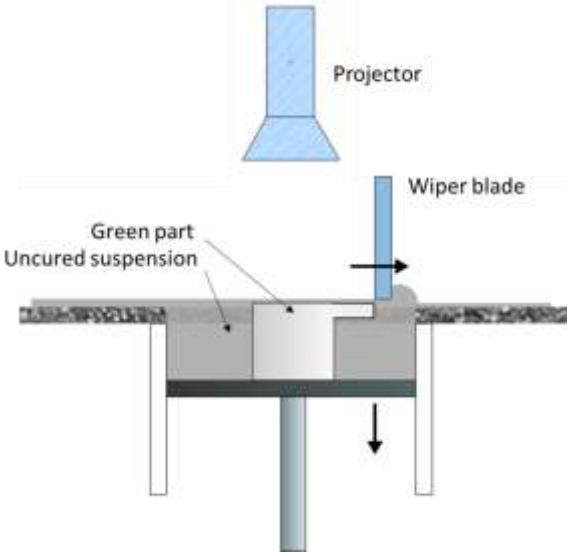

Figure 2 Sketch of the prototype machine setup.

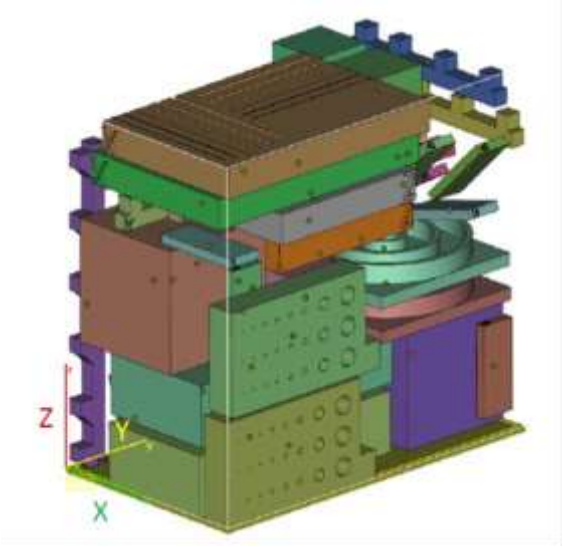

Figure 3 Nesting of benchmark parts in building volume

Results

Surface roughness

An Alicona confocal microscope was used to measure the surface roughness of as-sintered surfaces, built at varying angles as shown in Figure 4. Measurements were conducted on the top, bottom and side surfaces of each individual plate printed. The measured values for Ra are shown in Figure 5. This high level of surface quality correlates well with the expected strengths of VP. A slightly higher level of surface finish was measured on surfaces without layering influence (top and bottom surfaces of the plate printed at 0 degrees). All other plates will have layering influences and therefore a higher surface roughness. The side surface of the plated showed no clear sign of any layer influence.

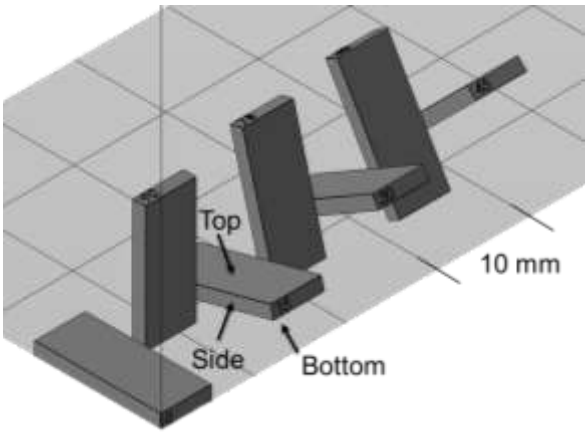

Figure 4 Roughness benchmark for determining surface finish of parts printed at various angles

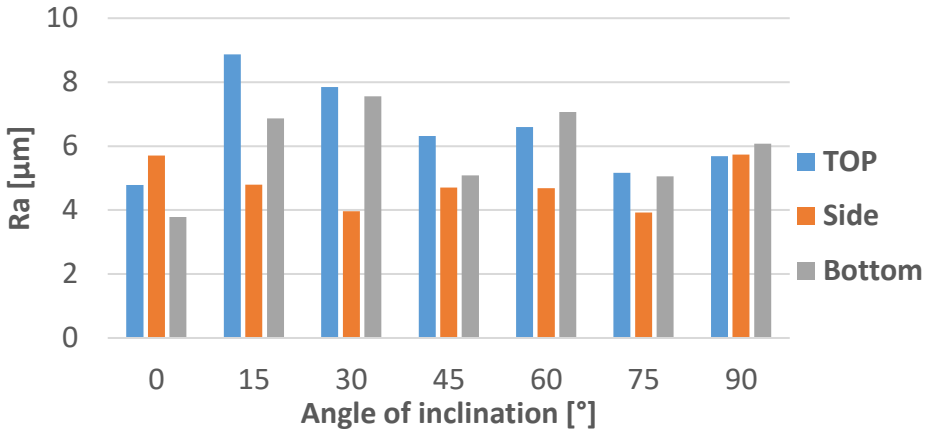

Figure 5 Surface roughness measurements

Part density

Part density was assessed using both Archimedes density (of 2 cubes and 3 cylinders) and optical microscopy of metallographic cut ups. Archimedes density measurements showed a density of 98.2 – 99.0 % based on a theoretical density of 7.87 g/cm^3 (as supplied by material data sheet from powder production). Metallographic analysis of the porosity area fraction showed a range of density between 94 – 95 % dense (Figure 6). The difference between the Archimedes method and the metallographic analysis requires further investigation.

Figure 6 Optical micrograph of sintered component (un-etched)

Mechanical Properties

Tensile testing was performed on specimens machined from cylinders built with dimensions 7 x 48 mm, (machined to gauge diameter of 2.5 mm, complying with ASTM E8 [9]). Results from testing are shown in Figure 7, together with a comparison of tensile properties with annealed wrought and LPBF processed 316L. LMM processed material shows comparable properties to wrought standard for 316L. This is due to the high density achieved and a fine austenite grain structure, developed by the sintering process. Compared to LPBF, the properties show an increased elongation at break, with a debit in yield stress and UTS. The LMM properties are likely to be isotropic, which is a benefit over LPBF, where material properties are typically anisotropic before heat treatment.

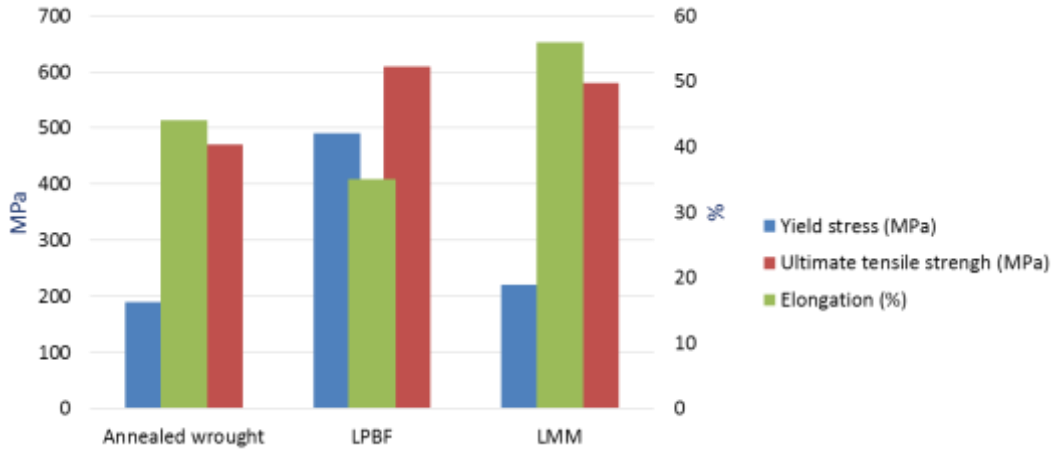

Figure 7 Comparison in tensile properties between annealed wrought [12], LPBF [13] and LMM processed 316L

Chemistry

LMM is a binder-based AM process and the metallic powder particles are in contact with carbon and hydrogen rich materials at elevated temperatures. Therefore it is necessary to understand whether this interaction has an influence on final part chemistry. Measurements of fully sintered parts were made through inert gas fusion (IGF) and spark atomic emission spectroscopy (AES) in accordance to ASTM E109-11 and E1086-14 respectively [10], [11]. The sintered part chemistry meets specification in all areas except a minor excess in carbon (Table 1). This is likely due to non-perfect debinding or through contamination of parts during sintering due to improper control of vaporized products in the sintering atmosphere. Both effects are controllable through full post processing development and improved contamination control in sintering.

Table 1 Sintered part chemistry compared to chemistry standard 316L stainless steel [14]

Element	Fe	Cr	Ni	Mo	Mn	Si	H	O	C	P	N	S
Standard	Bal	16-18.5	10-14	2-3	<2	<1	-	-	0.03	<0.045	-	<0.03
Measured	Bal	17.00	10.43	2.36	0.62	0.53	5 ppm	0.0011	0.05	0.018	0.0005	<0.004

Conclusion

Using the LMM process, sintered parts made of 316L stainless steel have been characterized in terms of surface roughness, mechanical properties, and chemistry. The results show great potential for the manufacturing of smaller, more complex parts, which require a high feature resolution and improved surface quality (Figure 8). Tensile properties observed in parts printed on the Hammer HD40 were shown comparable to wrought and exceeding cast with a yield stress, UTS and elongation of 224 MPa, 581 MPa & 56.9 % respectively. The presented process can be used to directly produce parts in a small-scale series or to manufacture prototypes prior to a MIM-based mass series production. Since the final geometry of the part is developed by means of a sintering process, similar microstructural properties compared to MIM can be achieved.

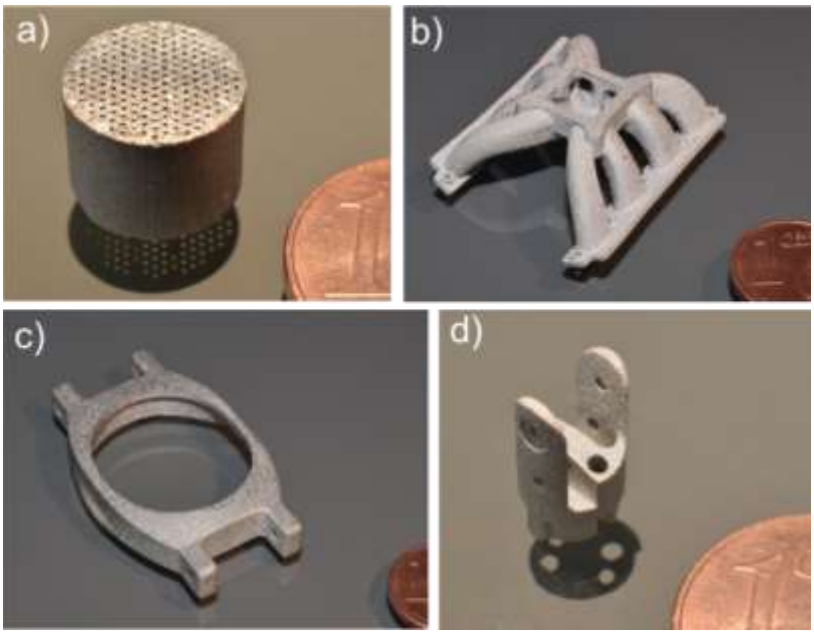

Figure 8 Sintered parts manufactured with LMM, a) Catalytic structure b) Intake manifold, c) Watch case, d) Hinge part

References

[1] "cubicure - Printing Performance Polymers." [Online]. Available: http://cubicure.com/. [Accessed: 07-May-2018].
[2] B. Steyrer, B. Busetti, G. Harakály, R. Liska, and J. Stampfl, "Hot Lithography vs. room temperature DLP 3D-printing of a dimethacrylate," *Addit. Manuf.*, vol. 21, pp. 209–214, May 2018.
[3] M. Schwentenwein and J. Homa, "Additive Manufacturing of Dense Alumina Ceramics," *Int. J. Appl. Ceram. Technol.*, vol. 12, no. 1, pp. 1–7, Jan. 2015.
[4] A. Gebhardt, *Generative Fertigungsverfahren: Additive Manufacturing und 3D Drucken für Prototyping - Tooling - Produktion*. Carl Hanser Verlag GmbH Co KG, 2013.
[5] "Home :: Lithoz." [Online]. Available: http://www.lithoz.com/. [Accessed: 07-May-2018].
[6] U. Scheithauer, E. Schwarzer, T. Moritz, and A. Michaelis, "Additive Manufacturing of Ceramic Heat Exchanger: Opportunities and Limits of the Lithography-Based Ceramic Manufacturing (LCM)," *J. Mater. Eng. Perform.*, vol. 27, no. 1, pp. 14–20, Jan. 2018.
[7] W. Harrer, M. Schwentenwein, T. Lube, and R. Danzer, "Fractography of zirconia-specimens made using additive manufacturing (LCM) technology," *J. Eur. Ceram. Soc.*, vol. 37, no. 14, pp. 4331–4338, Nov. 2017.
[8] P. J. Bartolo and J. Gaspar, "Metal filled resin for stereolithography metal part," *ResearchGate*, vol. 57, no. 1, pp. 235–238, Dec. 2008.
[9] ASTM Standard E8/E8M, 2106a, 'Standard Test Methods for Tension Testing of Metallic Materials', ASTM International, West Conshohocken, PA, DOI: 10.1520/ E0008_E0008M-16A.
[10] ASTM Standard E1019, 2011, 'Standard Test Methods for Determination of Carbon, Sulphur, Nitrogen, and Oxygen in Steel, Iron, Nickel and Cobalt Alloys by Various Combustion and Fusion Techniques' ASTM International, West Conshohocken, PA, DOI: 10.1520/E1019-11.
[11] ASTM E1086-14, Standard Test Method for Analysis of Austenitic Stainless Steel by Spark Atomic Emission Spectrometry, ASTM International, West Conshohocken, PA, 2014, www.astm.org.
[12] ASTM Standard F138, 2013, 'Standard Specification for Wrought 18Chromium-14Nickel-2.5Molybdenum Stainless Steel Bar and Wire for Surgical Implants (UNS S31673)', ASTM International, West Conshohocken, PA, DOI: 10.1520/F0138.
[13] R. plc, "Renishaw: Data sheets," *Renishaw*. [Online]. Available: http://www.renishaw.com/en/data-sheets-additive-manufacturing--17862. [Accessed: 07-May-2018].
[14] ASTM Standard A240/A240M, 2017, 'Standard Specification for Chromium and Chromium-Nickel Stainless Steel Plate, Sheet and Strip for Pressure Vessels and for General Applications' ASTM International, West Conshohocken, PA, DOI: 10.1520/A0240_A0240M-17.